LA-UR-01-6877

Title: **SINGLE CHAIN STOCHASTIC POLYMER MODELING AT HIGH STRAIN RATES**

Author(s): Eric N. Harstad, T-3
Francis H. Harlow, T-3
Howard. L. Schreyer, University of New Mexico

Submitted to: *2002 ASME Pressure* Vessels *& Piping Conference*
August 4-8, 2002
Vancouver, British Columbia, Canada

Proceedings of PVP'02
2002 ASME Pressure Vessels and Piping Conference
August 4-8, 2002, Vancouver, British Columbia, Canada

SINGLE CHAIN STOCHASTIC POLYMER MODELING AT HIGH STRAIN RATES

Eric N. Harstad*
Theoretical Division
Los Alamos National Laboratory
Mail Stop B216
Los Alamos, New Mexico 87545
Email: enh@lanl.gov

Francis H. Harlow
Theoretical Division
Los Alamos National Laboratory
Mail Stop B216
Los Alamos, New Mexico 87545
Email: fhharlow@lanl.gov

Howard L. Schreyer
Mechanical Engineering Department
University of New Mexico
Albuquerque, New Mexico, USA 87131
Email: schreyer@unm.edu

ABSTRACT

Our goal is to develop constitutive relations for the behavior of a solid polymer during high-strain-rate deformations. In contrast to the classic thermodynamic techniques for deriving stress-strain response in static (equilibrium) circumstances, we employ a statistical-mechanics approach, in which we evolve a probability distribution function (PDF) for the velocity fluctuations of the repeating units of the chain. We use a Langevin description for the dynamics of a single repeating unit and a Lioville equation to describe the variations of the PDF. Moments of the PDF give the conservation equations for a single polymer chain embedded in other similar chains. To extract single-chain analytical constitutive relations these equations have been solved for representative loading paths. By this process we discover that a measure of non-uniform chain link displacement serves this purpose very well. We then derive an evolution equation for the descriptor function, with the result being a history-dependent constitutive relation.

NOMENCLATURE

L Polymer chain length
N Number of repeating units in the polymer chain
P Probability density function
T Temperature
f Viscous drag parameter
k Boltzmann's constant
m Mass of a repeating unit in the polymer chain
s Order parameter describing the deformation within a chain
t Time
$A_i(t)$ Randomly fluctuating (thermal) force per unit mass
K_i Intermolecular force per unit mass
L_0 Initial polymer chain length
l_{c0} Initial length of a repeating unit in the chain
R_0 Initial polymer chain radius
u_i Velocity
u_0 Loading velocity
x_i Current spatial coordinate
X_i Material frame coordinate vector
κ Curvature
λ Stretch defined as L/L_0
$\dot{\lambda}$ Rate of stretch
Ψ Potential function
ρ Density
σ^{st} Surface tension stress
σ Stress
τ Traction

1 INTRODUCTION

Thermodynamically based solid polymer modeling traditionally has been applied with great success to quasi-static circumstances using the single chain model of Wang and Guth (1952) with homogenizations provide by James and Guth (1943) and more recently by Arruda and Boyce (1993). These approaches rely on describing the configurational entropy of the single chain, i.e., based on the chain elongation, the number of possible states the chain can occupy is used to determine the configurational entropy. The inherent assumption in this type

*Address all correspondence to this author.

of analysis is that the chain is in equilibrium. It is difficult to extend the thermodynamic approach to non-equilibrium circumstances. Since our interests lie in describing the chain behavior under both equilibrium and non-equilibrium(rate-dependent) circumstances we develop a physically based statistical model for the micromechanical motion of a chain.

We assume that a Langevin equation governs the motion of the repeating units of the chain. The Langevin equation includes the classical frictional-drag and random-thermal-fluctuation terms along with an intermolecular force term that accounts for the connection of each repeating unit to its neighbors in the chain. This Langevin equation is incorporated into an evolution equation for a Probability Distribution Function (PDF), and moments are taken in order to determine conservation equations for the chain.

We use the conservation equations in the numerical calculation of the single polymer chain behavior under several representative cases of rapid loading and unloading. One of the goals of these calculations is to determine the contribution that the single chain makes to the polymer network. The computational expense of solving the conservation equation for every chain in the network is not feasible, so that we determine a constitutive model that can reproduce the single chain behavior.

In a follow-on paper, we show the homogenization procedure, and how it builds on the single chain constitutive model derived in this work. A brief summary of the homogenization procedure is as follows: We account for the orientation of the chains and their evolution as the network is deformed. With the use of the single-chain constitutive equation, a response for each chain is determined, and through an upper-bound stress assumption a macro response is found by summing the individual responses. In addition, we introduce weighting functions and simplified initial chain geometries in order to reduce the number of chains that need to be simulated, which reduces significantly the computational expense associated with this type of homogenization. A full account of the homogenization procedure is given by Harstad (2001).

2 STOCHASTIC CONSERVATION EQUATIONS

In order to derive the stochastic conservation equations, we use a Liouville equation with a Langevin representation of the dynamics of each chain link. The Liouville equation describe how the PDF evolves in time. The PDF gives the probability per unit volume per unit velocity interval of finding a chain link with position $\mathbf{x}$, and velocity $\mathbf{u}$, at time t. The chain link is the repeating unit or micro-mechanical unit found in the chain. For this description, the appropriate Liouville equation is

$$\frac{\partial P}{\partial t}+\frac{\partial P\dot{x}_i}{\partial x_i}+\frac{\partial P\dot{u}_i}{\partial u_i}=0 \tag{1}$$

The Langevin equation is a momentum equation for each of the repeating units in the chain, which includes all the forces that are applied to the link. Classically, the Langevin equation has been used in the derivation of equations to describe Brownian motion (McQuarie,1973). For a single polymer chain imbedded in a medium of other polymer chains, several forces affect the motion of the chain as a whole, and the motion of the individual elements. There are viscous forces that describe the frictional force or drag. The thermal force due to the vibrations of the repeating units in the chain must be considered. Also, the intermolecular force that physically holds the repeating units into a chain affects the motion of the chain, especially near the limits of large extension. All of these forces are included in our form of the Langevin equation (Uhlenbeck and Ornstein, 1930), which governs the motion of each element of the chain

$$\frac{du_i}{dt}=-fu_i+A_i(t)+K_i(\mathbf{x}) \tag{2}$$

f is the drag coefficient, $A_i(t)$ is the randomly fluctuating (thermal) Note that for the frictional drag the lowest order approximation (linear) is used and, if needed, higher order terms can be considered. We impose the following assumptions on the statistics of the randomly fluctuating term. The term has a zero mean sum, and the product of two of the terms only has value if the times are close to each other within the terms, and the statistics of the term are Gaussian. The Gaussian assumption would appear to contradict our goal to capture the non-equilibrium effects of high-strain-rate deformations. However, we indicate how this assumption can be relaxed through a Chapman-Enskog approach (Harstad,2001). Our current postulate, however, is that the dominant effects of non-equilibrium are produced by transient departure of the chain from uniformity of link spacing.

The conservation equations are found by inserting the Langevin equation into the Liouville equation and taking moments over a sphere of radius r in velocity space. When taking these moments, we assume that P goes to zero sufficiently fast enough that $r^4P\to 0$ as $r\to\infty$. This is to say that the probability of having a large velocity vanishes much faster than r^4. With this assumption of the statistics of P, the first through third moments give the conservation equations for mean mass, momentum, and energy (Q_{ij} Transport) equations at any point in the chain.

$$\frac{\partial\overline{\rho}}{\partial t}+\frac{\partial\overline{\rho}\,\overline{u}_i}{\partial x_i}=0 \tag{3}$$

$$\frac{\partial\overline{\rho}\,\overline{u}_i}{\partial t}+\frac{\partial\overline{\rho}\,\overline{u}_i\overline{u}_j}{\partial x_j}+\frac{\partial Q_{ij}}{\partial x_j}=\overline{\rho}(\overline{K_i}-f\overline{u}_i) \tag{4}$$

$$\frac{\partial Q_{ij}}{\partial t} + \frac{\partial \overline{u}_k Q_{ij}}{\partial x_k} + \frac{\partial Q_{ijk}}{\partial x_k} =$$
$$-2fQ_{ij} + \overline{\rho}\frac{2kTf}{m}\delta_{ij} - Q_{jk}\frac{\partial \overline{u}_i}{\partial x_k} - Q_{ik}\frac{\partial \overline{u}_j}{\partial x_k} \quad (5)$$

In the above equations variables with an overbar denote mean quantities, variables with a prime denote fluctuating quantities, such that the overbar plus the fluctuating quantity equals the instantaneous quantity. The variables not previously defined are as follows: $Q_{ij} \equiv \int u_i' u_j' P dV_{\mathbf{u}}$ and $Q_{ijk} \equiv \int u_i' u_j' u_k' P dV_{\mathbf{u}}$, in which $dV_{\mathbf{u}}$ is a volume element in u_i space.

3 SINGLE CHAIN SIMULATIONS

3.1 REDUCTION OF THE EQUATION SET

Assume that the chains deform in an incompressible manner ($\overline{\rho}$ = constant), which is consistent with observations of viscoelastic polymer behavior at low to moderate strain rates. Then,

$$\frac{\partial \overline{u}_i}{\partial x_i} = 0 \quad (6)$$

and

$$\overline{\rho}\frac{\partial \overline{u}_i}{\partial t} + \overline{\rho}\,\overline{u}_j\frac{\partial \overline{u}_i}{\partial x_j} + \frac{\partial Q_{ij}}{\partial x_j} = \overline{\rho}(\overline{K_i} - f\overline{u}_i) \quad (7)$$

Next, assume that the stochastic variable $\overline{K_i}$ is derivable from a potential i.e.,

$$\overline{\rho}\,\overline{K_i} = -\frac{\partial \Psi}{\partial x_i}$$

The momentum equations become

$$\overline{\rho}\frac{\partial \overline{u}_i}{\partial t} + \overline{\rho}\,\overline{u}_j\frac{\partial \overline{u}_i}{\partial x_j} = -\frac{\partial \Psi}{\partial x_i} - \overline{\rho} f\overline{u}_i \quad (8)$$

With incompressibility the divergence of the momentum equation results in a Poisson equation for the potential function.

$$\overline{\rho}\frac{\partial \overline{u}_j}{\partial x_i}\frac{\partial \overline{u}_i}{\partial x_j} = -\frac{\partial^2 \Psi}{\partial x_i x_i} \quad (9)$$

If we neglect time and spatial variations in Eq. (5), Q_{ij} is exactly constant,

$$Q_{ij} = \frac{\overline{\rho} kT}{m}\delta_{ij} \quad (10)$$

3.2 BOUNDARY CONDITIONS

We refer to the configuration of the chain as a cloud. This cloud represents the portion of a polymer chain that is between tie-points. Note that the cloud is a stochastic concept; at any instant some elements may lie briefly outside the cloud boundary. It is the stochastic cloud that is considered to be incompressible. For the reduced equation set, boundary condition expressions are developed. These conditions provide the link between the applied forces on the boundary and the internal variables such as Ψ and Q_{ij}. Derivation of the boundary conditions is accomplished by looking at the change in momentum due to the applied forces on the surface of the chain cloud

$$\frac{\Delta \text{momentum}}{\Delta t} = \sum \text{external forces} + \sum \text{internal forces} \quad (11)$$

Each force is the product of a traction, τ_i, and an area. These forces are shown in Fig. 1. In the limit in which the dimensions of the slice go to zero, the mass also goes to zero, so that causes the left side of Eq. (11) to go to zero. Because the change in momentum must be bounded, the right side of Eq. (11) must go to zero. A tangential force balance shows that the left and right forces cancel with one another. The resulting force balance in the normal direction results in

$$\tau_i^{\text{external}} A^{\text{external}} + \tau_i^{\text{internal}} A^{\text{internal}} = 0 \quad (12)$$

In addition, in the limit in which the thickness of the slice is infinitesimally small, the external and internal areas are the same and we can directly relate the tractions to one another,

$$\tau_i^{\text{external}} = \tau_i^{\text{internal}} \quad (13)$$

The internal traction is given by the normal component of the sum of the potential function and Q_{ij} The external traction is composed of two components, an applied traction that occurs at tie-points and a traction due to the interactions of the chain with

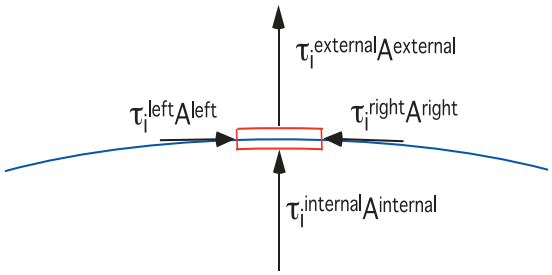

Figure 1. FORCES ON A POINT ON THE SURFACE CONTAINING AN ENTIRE CHAIN.

other surrounding chains:

$$\tau_i^{\text{external}} = \tau_i^{\text{applied}} + \tau_i^{\text{interactions}} \tag{14}$$

We postulate that interaction with the surrounding chains can be represented by a surface tension force. In other words, the chain keeps its cloud shape due to encasement by surrounding chains. This stress is represented mathematically in the standard form

$$\sigma^{st} = C\kappa, \tag{15}$$

in which $C = \frac{\overline{\rho}kT}{m} l_{c0}$ is a constant with units of force per unit length, and the curvature, $\kappa = -\frac{\partial n_i}{\partial x_i}$. In terms of the two principal curvatures, the surface tension stress is

$$\sigma^{st} = \frac{\overline{\rho}kT}{m} l_{c0} \left(\kappa_1 + \kappa_2\right), \tag{16}$$

thus

$$\tau_i^{\text{interactions}} = -\sigma^{st} n_i \tag{17}$$

With this result and the equilibrium value for $Q_{ij} = \frac{\overline{\rho}kT}{m}\delta_{ij}$, we can solve for the applied traction, from which we hereafter omit the superscript on the traction symbol;

$$\tau_i = \left\{ \frac{\overline{\rho}kT}{m} \left[1 + l_{c0} \left(\kappa_1 + \kappa_2\right)\right] + \Psi \right\} n_i \tag{18}$$

3.3 ELLIPSOIDAL DEFORMATION

The equations for determining the behavior of a polymeric chain with arbitrary shape are given in Section 2. To demonstrate the validity of this model for the case of static deformation, we consider its application for a single chain in the configuration of an axisymmetric ellipsoid. This shape allows for the investigation of the traction-stretch relationship in a geometry with a simple expression for the surface curvature. The configuration of the chain and its deformed shape are shown in Fig. 2. We assume that during pulling on the tie-points to the single chain the cloud maintains the configuration of the ellipse. The applied tractions are partially balanced through the curvatures of the ellipse as shown in Eq. (18). We determine the curvatures through the geometric description of the ellipse. The locations on the ellipse where we need the curvatures are at the point of loading, and where it meets the vertical axis. The radius of the surface in polar coordinates is

$$r_s = \frac{ab}{\sqrt{a^2 \sin^2\theta + b^2 \cos^2\theta}} \tag{19}$$

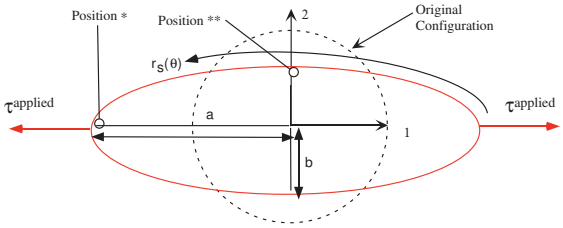

Figure 2. LOADING PATH IMPOSED ON THE ELLIPSOID.

The curvature κ in an $r-z$ cut of the surface is (Zwillinger, 1996)

$$|\kappa| = \frac{\left[r_s^2 + 2\left(\frac{dr_s}{d\theta}\right)^2 - r_s \frac{d^2 r_s}{d\theta^2}\right]}{\left[r_s^2 + \left(\frac{dr_s}{d\theta}\right)^2\right]^{3/2}} \tag{20}$$

There are two principal orthogonal curvatures at every point on the surface of the ellipsoid. At angles of 0 and π, the two principal curvatures are the same

$$\kappa_1, \kappa_2 = -\frac{a}{b^2} \tag{21}$$

For angles of $\pi/2$ and $3\pi/2$, the curvature in the plane shown in Fig. 2 is

$$\kappa_1 = -\frac{b}{a^2} \tag{22}$$

In the orthogonal plane, the cross section of the ellipsoid at position $**$ is a circle of radius b, so that the component of curvature is

$$\kappa_2 = -\frac{1}{b} \tag{23}$$

These expressions for curvature based on the ellipsoid parameters a and b can be converted to expressions based on the stretch, λ, through the relations

$$\lambda_1 = \frac{a}{a_o}, \lambda_2 = \frac{b}{b_o}, \tag{24}$$

in which the subscript, o, refers to the undeformed sphere. The incompressibility assumption provides a constraint on the values of a and b. In conserving the volume of the ellipse, the following must be satisfied:

$$\lambda_2 = \frac{1}{\sqrt{\lambda_1}} \tag{25}$$

At the point on the surface labeled position $*$, the applied traction is found from Eq. (18)

$$\tau_1 = \left(\frac{\overline{\rho} kT}{m} + \Psi - \frac{\overline{\rho} kT}{m} l_{c0} \frac{2a_o}{b_o^2} \lambda_1^2 \right) n_1 \tag{26}$$

At the surface in position $**$ the traction is purely in the vertical direction. For this position there is no applied stress so that

$$\tau_2 = 0 = \left[\frac{\overline{\rho} kT}{m} + \Psi + \frac{\overline{\rho} kT}{m} l_{c0} \left(\frac{b_o}{a_o^2} \lambda_1^{-3/2} + \frac{1}{b_o} \lambda_1^{1/2} \right) \right] n_2 \tag{27}$$

This enables us to solve for the potential, Ψ, which is constant throughout the interior for the quasi-static case and given by

$$\Psi = -\frac{\overline{\rho} kT}{m} \left[1 + l_{c0} \left(\frac{b_o}{a_o^2} \lambda_1^{-3/2} + \frac{1}{b_o} \lambda_1^{1/2} \right) \right] \tag{28}$$

This is substituted back into the relationship for the traction in the horizontal direction

$$\tau_1 = \frac{\overline{\rho} kT}{m} l_{c0} \left(-\frac{1}{b_o} \lambda_1^{1/2} - \frac{b_o}{2a_o^2} \lambda^{-3/2} + \frac{2a_o}{b_o^2} \lambda_1^2 \right) n_1 \tag{29}$$

so that the normal stress can be determined from $\tau_i = \sigma_{ij} n_j$ to give

$$\sigma_{11} = \frac{\overline{\rho} kT}{m} l_{c0} \left(-\frac{1}{b_o} \lambda_1^{1/2} - \frac{b_o}{2a_o^2} \lambda^{-3/2} + \frac{2a_o}{b_o^2} \lambda_1^2 \right) \tag{30}$$

Because the undeformed geometry is a sphere, the parameters a_o and b_o equal the initial radius r_0, so that Eq. (30) becomes

$$\sigma_{11} = \frac{\overline{\rho} kT}{m} \frac{l_{c0}}{r_0} \left(-\lambda_1^{1/2} - \lambda_1^{-3/2} + 2\lambda_1^2 \right) \tag{31}$$

The behavior of this equation is illustrated by choosing material parameters as: $R_0 = 3 \times 10^{-7}$m, $T = 300$ K, $\overline{\rho} = 1088$ kg/m^3, $m = 3 \times 10^{-25}$kg, and $l_{c0} = 1 \times 10^{-8}$m and plotting the resulting stress-stretch relation. Figure 3 shows a comparison of our micro-mechanical model with these parameters to the Mooney-Rivlin model for uniaxial stress (Treloar, 1975). We see that there is a close correlation between the response of the two models. It is also observed that as the stretch gets large, the stress varies in proportion to λ_1^2.

For large stretches, Eq. (31) must be modified by the constraint of finite chain extensibility, in which all of the links of the chain are essentially in a straight line and further tensile deformation must overcome the force required to physically separate the repeating units in the chain. The finite chain extensibility has been included in equilibrium thermodynamic models starting with the development of James and Guth (1943). While we realize that this is an important feature of polymer behavior at deformations near the locking stretch, as a first attempt at modeling the single chain, we do not include it in this paper. This limits us to only considering problems in which the finite extensibility does not dominate the behavior.

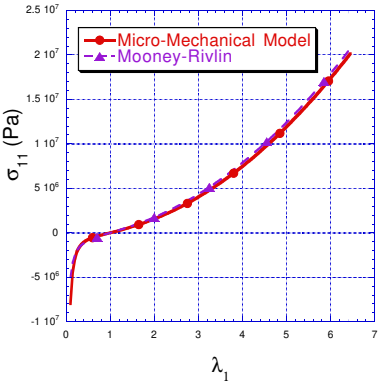

Figure 3. COMPARISION OF THE CURRENT MICRO-MECHANICAL MODEL WITH THE MOONEY-RIVLIN MOCEL FOR UNIAXIAL STRESS.

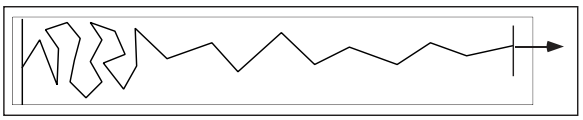

Figure 4. NON-UNIFORM LINK DISTRIBUTION FROM RAPID EXTENSION AT ONE END.

3.4 LOADING PATHS AND PREDICTED BEHAVIOR

The essence of our work is to demonstrate that a single chain imbedded in a random array of other chains responds to transient deformations through the development of variations in relative displacement of its links; see Fig. 4. This non-uniformity is continuously created during the deformation, but also is continuously tending to relax to uniformity. We show the effects of these competing processes for several types of loading paths using both analytical and numerical methods. Under several simplifying assumptions, the full equation set can be reduced to a one-dimensional partial differential equation. Numerical solutions at different stretch rates and for different loading paths provide descriptions of macroscopic chain behavior. i.e. the end stresses as functions of the overall stretch. The goal is to use these solutions to find a constitutive law, based on the available macroscopic single-chain variables, that represents the simula-

tions for simple loads.

In order to investigate the properties of the chain behavior, a one-dimensional equation of motion is determined from the three-dimensional form(Eq. (8)). In the axial direction the equation of motion is

$$\frac{\partial u}{\partial t} + u\frac{\partial u}{\partial x} = -\frac{1}{\overline{\rho}}\frac{\partial \Psi}{\partial x} - fu \tag{32}$$

Several assumptions have been imposed in the reduction to this form:

1. The material is incompressible
2. The deformation of the chain cloud is axisymmetric
3. The only interaction in the radial direction is with other chains. i.e. the externally applied loads are only in the axial direction.
4. The axial velocity is independent of radius, i.e. $u = u(x,t)$.

The one dimensional mass equation is

$$\frac{\partial R^2}{\partial t} + \frac{\partial R^2 u}{\partial x} = 0 \tag{33}$$

With the third assumption, the potential Ψ in Eq.(18)) becomes

$$\Psi = -\frac{\overline{\rho} kT}{m}\left[1 + l_{c0}(\kappa_1 + \kappa_2)\right] \tag{34}$$

For the assumed ellipsoidal shape, the curvatures to lowest order in the $r-z$ and $r-\theta$ directions are

$$\kappa_1 = \frac{\partial^2 R}{\partial x^2} \text{ and } \kappa_2 = \frac{1}{R}, \tag{35}$$

respectively. With the use of the previous assumptions, the curvatures, and when higher-order terms are neglected, the momentum equation is

$$\frac{\partial u}{\partial t} + u\frac{\partial u}{\partial x} = \frac{1}{\overline{\rho}}\frac{\partial \sigma}{\partial x} - fu \tag{36}$$

in which $\sigma = E_0(\lambda - 1)$; $E_0 = \frac{\overline{\rho} kT l_c}{R_0}$.

We consider 4 loading cases for the single chain; see Fig 5.

Loading One: Constant velocity then hold

$$u(L,t) = \begin{cases} u_0 & : \quad t < t_1 \\ 0 & : \quad t \geq t_1 \end{cases}$$

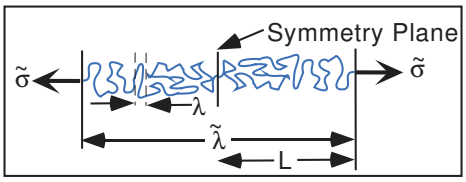

Figure 5. SINGLE CHAIN MACROSCOPIC STRESS AND STRETCH ASSOCIATED WITH THE END POINTS OF THE CHAIN.

Loading Two: Constant velocity, then reverse the direction of the velocity

$$u(L,t) = \begin{cases} u_0 & : \quad t < t_1 \\ -u_0 & : \quad t \geq t_1 \end{cases}$$

Loading Three: Constant velocity, hold, then reverse

$$u(L,t) = \begin{cases} u_0 & : \quad t < t_1 \\ 0 & : \quad t_1 \leq t < t_2 \\ -u_0 & : \quad t \geq t_2 \end{cases}$$

Loading Four: Sinusoidal loading

$$u(L,t) = u_0 \sin\left(\frac{2\pi t}{t_f}\right)$$

in which t_f is the period of oscillation.

We use these loading cases to examine the single chain response under rate dependent circumstances.

3.5 MATERIAL PARAMETERS

Material parameters used in this investigation are chosen to be within the range of relevant polymers, such as plasticized estane, rather than to fit the properties of any one material. Some parameters, such as initial modulus, come from true macroscopic (multi-chain) tests. The relationship of these parameters to their equivalent single chain parameters is unknown, but we work under the assumption that the values are similar. The parameters used in the simulations are: $T = 300\text{K}$, $\rho_0 = 1190\,\text{kg/m}^3$, $m = 100\,\text{AMU}$, $l_{c0} = 0.001\mu\text{m}$, $f = 4 \times 10^{10}\text{kg}/(\text{s m}^2)$, $k = 1.3792 \times 10^{-23}\text{J/K}$, $L_0 = 100\mu\text{m}$, and $R_0 = 100\mu\text{m}$.

3.6 MACROSCOPIC PROPERTIES

Several macroscopic properties of a single chain are useful in describing the mechanical response, which guides the development of a single chain constitutive model. These include $\tilde{\lambda}$, $\dot{\tilde{\lambda}}$,

σ and a non-equilibrium parameter s. These are not the continuum level macroscopic properties, but the properties describing the overall state of a single chain.

The first two variables are the average stretch and stretch rate experienced by the entire chain.

$$\tilde{\lambda} = \frac{1}{L_0}\int_0^{L_0}\left(\frac{\partial x}{\partial X}\right)dX \tag{37}$$

$$\dot{\tilde{\lambda}} = \frac{d\tilde{\lambda}}{dt} \tag{38}$$

The macroscopic stress, σ, is identified as the current stress at the ends of the chain. We can consider symmetric deformation about the center of the chain without loss of generality, so the stress at both ends of the chain is identical, and the tractions differ by a sign. This is shown in Fig. 5. In addition, it can be shown that the average stretch for the chain and the half chain are identical. This type of symmetric deformation allows for calculations involving half of the chain.

In the determination of a suitable constitutive model, a non-equilibrium descriptor variable is developed to show the state of non-uniformity of the chain-link displacement. The non-equilibrium descriptor, s, is the following measure of the non-uniformity of the chain deformation.

$$s = \sqrt{\int_0^{L_0}\frac{1}{L_0}\left(\frac{\partial x}{\partial X} - \frac{1}{L_0}\int_0^{L_0}\frac{\partial x}{\partial X}dX\right)^2 dX} \tag{39}$$

For quasi-static situations, s is very small. In high stretch rate circumstances, one end of the chain may be deforming rapidly, whereas the other end has barely moved. This gives a large value for s. The quantity s can also be thought of as a measure of how much viscous stress is stored in the chain. As the viscous stress in the chain relaxes, the value of s drops and vice-versa. A major postulate of our investigation is that the strain-rate effects for many circumstances of interest can be adequately described by the behavior of this single non-equilibrium descriptor.

In order to use the constitutive model for general problems, it is necessary to know the evolution of this descriptor. No simple equation exists that accurately describes its evolution. Therefore, in addition to the development of the constitutive model, the non-equilibrium descriptor is also modeled and compared against the exact value.

3.7 SIMULATIONS AND RESULTS

We use the form of a linear elastic stress-stretch relationship without the finite extensibility term to describe the behavior of the links in the chain, and show results for each of the four loadings. The results shown are stress versus time or stretch and the time evolution of the non-equilibrium parameter. The input parameters for each loading are similar, with the following variations in velocity.

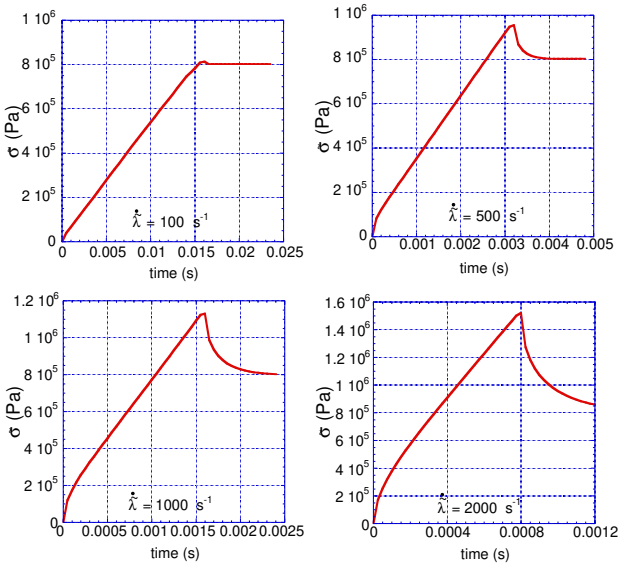

Figure 6. STRESS VERSUS TIME FOR LOADING TYPE ONE.

$$u_0 = (0.01, 0.05, 0.10, 0.2)\ \text{m/s} \tag{40}$$

These variations in velocity correspond to the following macroscopic values of stretch rate.

$$\dot{\tilde{\lambda}} = (100, 500, 1000, 2000)\ \text{s}^{-1} \tag{41}$$

For comparison purposes, each type of loading was calculated to the same maximum value of stretch. Due to the variation in the stretch rate for the sinusoidal loading, the end time was adjusted to obtain the same value of maximum stretch.

3.7.1 LOADING ONE We study the behavior of the chain at four different strain rates for the extend and hold loading. The results for the stress as a function of time for these rates are shown in Fig. 6. After the stretch rate goes to zero, we get a rate dependent response that decays to the elastic response. Figure 7 shows how the non-equilibrium parameter evolves in time. For low strain rates, the value of s, as calculated by a finite-difference approximation to Eq. (39), increases in a bilinear fashion and then decays to near zero after the stretch rate goes to zero.

3.7.2 LOADING TWO The results from this loading are valuable because they give the material response to an even

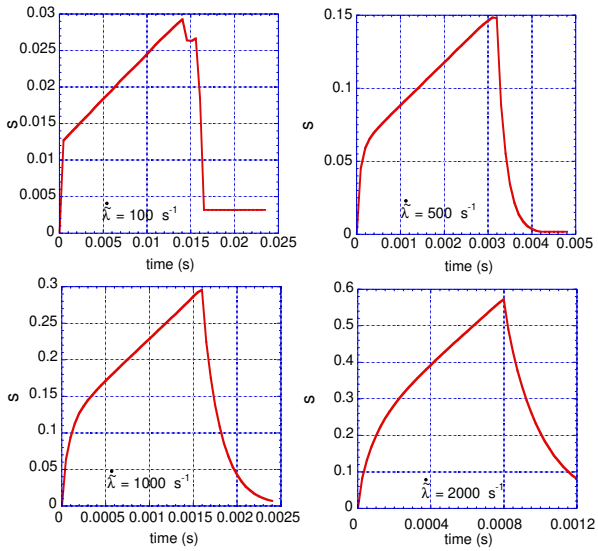

Figure 7. s VERSUS TIME FOR LOADING TYPE ONE.

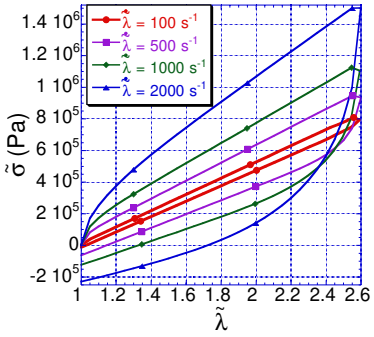

Figure 8. STRESS VESUS STRETCH FOR LOADING TYPE TWO.

more severe discontinuity in the stretch rate than occurred from loading one. The effect that this type of discontinuity has on the material response is important for the simulation of impact tests and other mid-rate stretch experiments. Examples of these experiments the Hopkinson bar or Taylor cylinder impact test. It is important to be able to model experiments of this type because they provide useful measurements of the material behavior under rate-dependent conditions.

The results for the stress as a function of stretch for various stretch rates are shown in Fig. 8. This figure shows that we obtain classic hysteresis loops. The magnitude of the hysteresis displacement increases with increasing rate of stretch.

Figure 9 shows how s evolves with time for the load reversal, as calculated by a numerical integration of Eq. (39). It can be seen that the reversal of the loading manifests itself by briefly restoring order to the chain, but then the chain begins to get more non-uniform as it piles up against the right side. Eventually, the entire chain commences to become increasingly more uniform and the value of s decreases. The behavior of s depends on the deformation wave speed, and rate of loading, and the length of

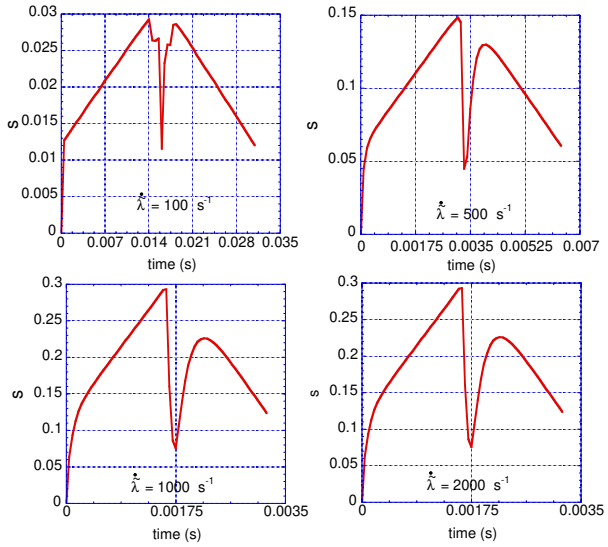

Figure 9. s VERSUS TIME FOR LOADING TYPE TWO.

the chain. For the slowest loading rate (100 s^{-1}), a sharp drop in s is seen at around 0.014 seconds. The reversal time for this case was 0.016 seconds. This result indicates that the loading speed was slow enough that the deformation wave propagated nearly across to the other end of the chain, and hence the deformation was becoming more uniform. The other five cases do not show this behavior because the loading is occurring at a much faster rate.

3.7.3 LOADING THREE For this loading we extend the chain, hold it, then recompresses. This allows us to combine the effect of rapid loading with the decay in stress for a static strain rate, as in loading two, and then to investigate the effects on unloading to see if the history of chain deformation was a significant effect. Figures 10 and 11 show stress versus time and s versus time respectively.

From the stress plots, a rate dependent rise is followed by a decay back to the elastic solution, and finally by a rate dependent decrease in stress. This loading illustrates the complexities that can occur as the chain returns to equilibrium. The relative intervals of extension, holding, and returning are the same in all of the calculations. For slow stretch rates, the non-equilibrium parameter has time to fully decay to a value consistent with a uniform deformation. At higher rates, the chain cannot fully recover in the constant strain portion of the loading before it is reloaded.

3.7.4 LOADING FOUR In this loading, the motion of the right end of the chain is sinusoidal, through one complete period of oscillation. The results for the stress as a function of stretch for various stretch rates is shown in Fig. 12. We see that the response is similar to that of the loading rate reversal, except that with the smooth variation in stretch rate for the sinusoidal loading, the mechanical response is much smoother. The non-

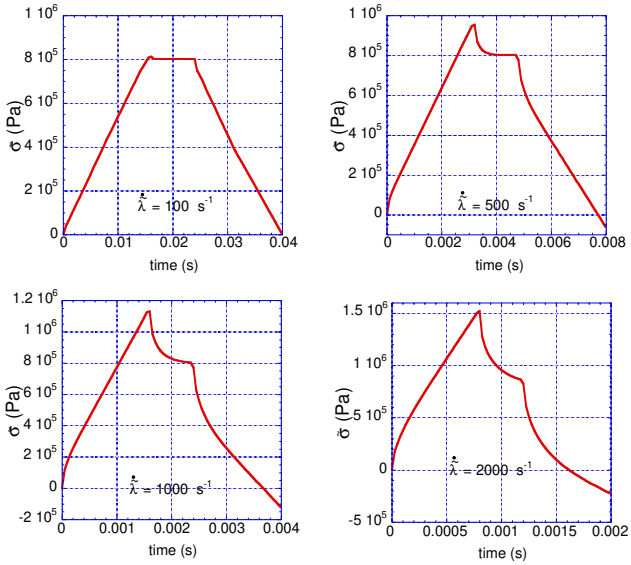

Figure 10. STRESS VERSUS TIME FOR LOADING TYPE THREE.

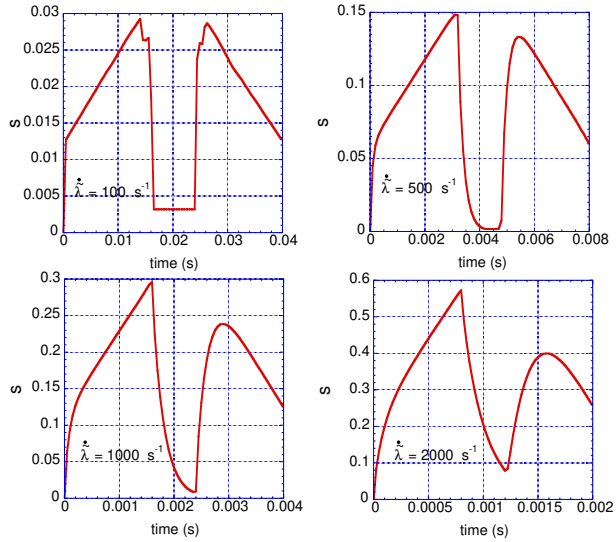

Figure 11. *s* VERSUS TIME FOR LOADING TYPE THREE

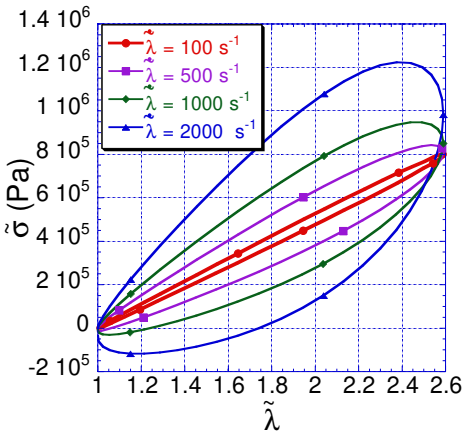

Figure 12. STRESS VERSUS STRETCH FOR LOADING TYPE FOUR.

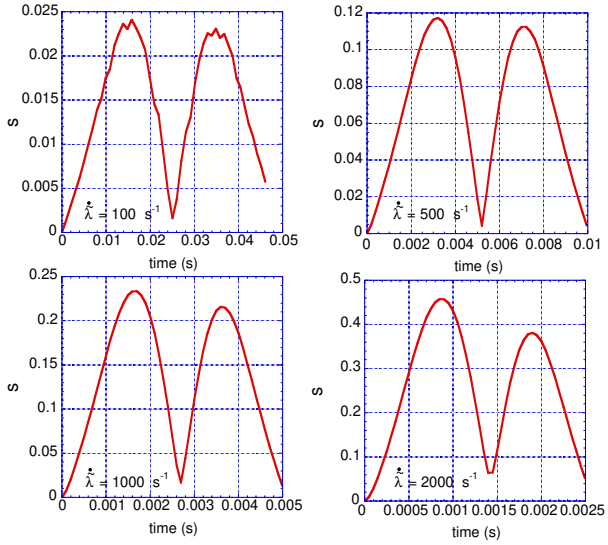

Figure 13. *s* VERSUS TIME FOR LOADING TYPE FOUR.

equilibrium parameter behavior in Fig. 13 shows that decreasing the stretch rate going into the load reversal and the slow ramping after the reversal allows for s to return to almost its equilibrium value for all of the calculations (i.e. $s = 0$). The evolution of s is almost "self-similar" among these runs, indicating that the asymmetries occurring with the other loadings are due to discontinuities in the stretch rate.

4 CONSTITUTIVE EQUATION DEVELOPMENT

From the differential description of single chain behavior presented in Eq. (36), we wish to extract a relatively simple model in which the macro stress in the chain, $\tilde{\sigma}$, can be described as a function of the overall stretch, $\tilde{\lambda}$, stretch rate, $\dot{\tilde{\lambda}}$, and the non-equilibrium descriptor, s.

The determination of a suitable form for this constitutive relation is based on the results of detailed numerical solutions of the full equation. We use a purely linear form for stress as a function of stretch, and limit ourselves to deformations in which the finite extensibility is not important. There are three main phases of deformation for which we develop the model. These phases are extension at various stretch rates, holding at constant deformation leading to decay to the elastic solution, and cyclic loading. The proposed constitutive equation is based on the postulate of a single non-equilibrium descriptor, which means that there is no guarantee that it will work for all stretch rates, stretches, and loading paths.

A relatively simple form that works well for stretch rates in the interval $10\ \mathrm{s}^{-1} - 2000\ \mathrm{s}^{-1}$ for the loading histories examined

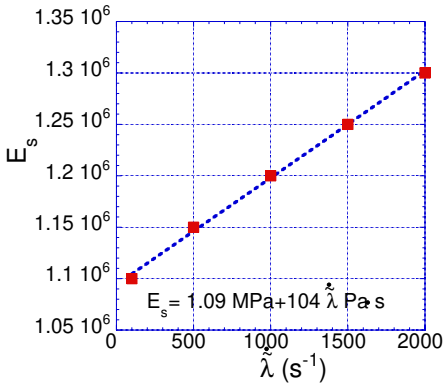

Figure 14. LINEAR FIT OF E_s VERSUS STRETCH RATE.

in Section 3.7 is

$$\sigma = E_e\left(\tilde{\lambda} - 1\right) + E_s s \tag{42}$$

$$E_s = C_s(E_{s0} + E_{s1}\left|\dot{\tilde{\lambda}}\right|) \tag{43}$$

$$C_s = \begin{cases} 1 & : \quad \dot{\tilde{\lambda}} \geq 0 \\ -1 & : \quad \dot{\tilde{\lambda}} < 0 \end{cases} \tag{44}$$

The numerical validation of this model was done with material values given in Section 3.5.

In order to fit this model to the calculation, the constants E_{s0} and E_{s1} must be determined by the response predicted by the numerical solutions of Eq. (36). By looking at extension runs at several stretch rates, the value of E_s can be computed from the inverted constitutive model for E_s, i.e.

$$E_s = \left[\sigma - E_e\left(\tilde{\lambda} - 1\right)\right]/s \tag{45}$$

A value for E_s was determined for each stretch rate and then a linear fit to Eq. (43) was performed in order to find the value of the unknown constants, E_{s0} and E_{s1}. The values of E_s versus stretch rate are shown in Fig. 14. From this figure, the values of the constants can be determined:

$$E_{s0} = 1.09 \times 10^6 \text{ Pa}$$
$$E_{s1} = 104 \text{ Pa} \cdot \text{s}$$

With these constants, we compare the constitutive-model results with those obtained from full numerical solutions of Eq. (36) for various stretch rates and loading paths. Identical loadings with the same input parameters as in Section 3.7 were used in these comparisons. Figures 15 - 18 show the comparisons of the mechanical response for the calculation and the model for four

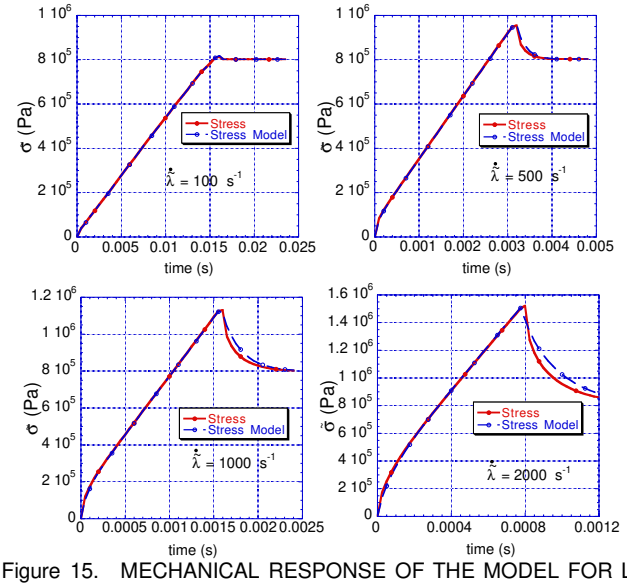

Figure 15. MECHANICAL RESPONSE OF THE MODEL FOR LOADING TYPE ONE.

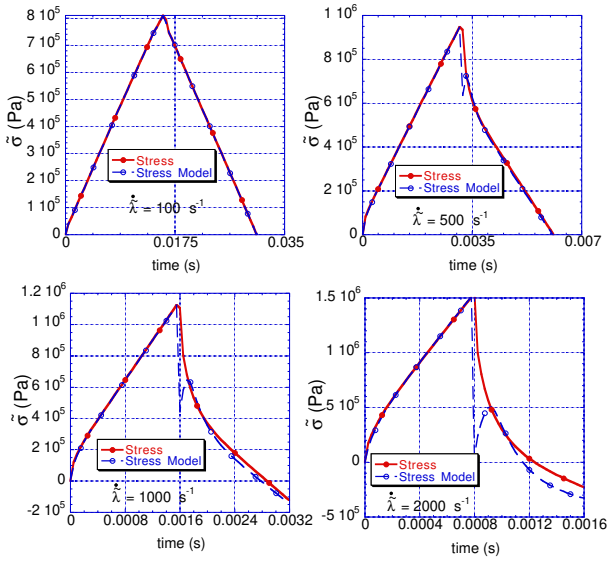

Figure 16. MECHANICAL RESPONSE OF THE MODEL FOR LOADING TYPE TWO.

different loading paths that are described in Section 3.4. We observe from these comparisons that the results from the model and the calculations indicate close agreement, but that as the stretch rate increases, the model deviates somewhat from the calculation. This is particularly noticeable in the stretch rate reversal loading, shown in Fig. 16. The discontinuity in the stretch rate, as occurs in loading two, is an extreme challenge for any model to describe. There are several possible ways to remedy this discrepancy. One way could be the incorporation of higher time derivatives of the stretch rate, $\dot{\tilde{\lambda}}$, i.e. to include terms proportional to $\ddot{\tilde{\lambda}}$ and/or $\dddot{\tilde{\lambda}}$; however, there is concern as to whether this pro-

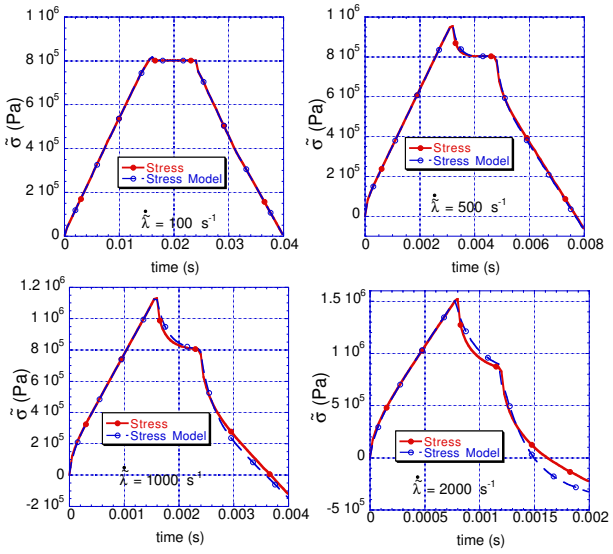

Figure 17. MECHANICAL RESPONSE OF THE MODEL FOR LOADING TYPE THREE.

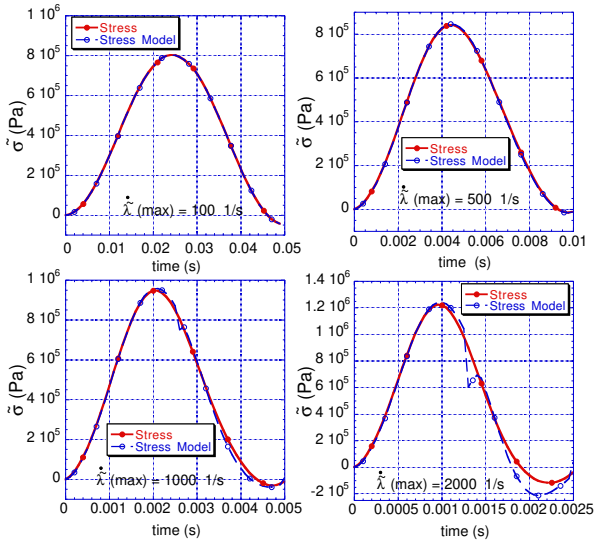

Figure 18. MECHANICAL RESPONSE OF THE MODEL FOR LOADING TYPE FOUR.

cess would converge. Another avenue of pursuit is to introduce one or more additional descriptors by which to more accurately characterize the non-equilibrium configuration of the chain. Because the simple model nevertheless works well for rather complicated loading histories, we believe that the next steps of the investigation should be to compare the current model with experimental data, before developing more complicated approaches. In order make this comparison, the model has been implemented into a homogenization scheme. We conclude that the proposed model works well for stretch rates up to around 10^3 s^{-1}, but may need to be modified for larger rates.

5 NON-EQUILIBRIUM DESCRIPTOR DEVELOPMENT

Section 4 describes the single-chain constitutive model that depends on the behavior of the non-equilibrium descriptor s. This macrovariable varies as a function of the variation of deformation within the chain. In the calculations, the value of the descriptor can be obtained at any time. The goal of this section is to eliminate having to perform the micro-mechanical calculations to obtain s for use in the constitutive model. For this reason, we develop an evolution equation for the non-equilibrium parameter.

5.1 ANALYTICAL DERIVATION OF THE EVOLUTION OF s

To derive an evolution equation for s, we assume a polynomial series to describe the local behavior of λ, and truncate the series beyond the quartic term. The odd terms are eliminated by the assumption of a symmetric deformation about the mid-point in the chain ($X = 0$),

$$\lambda(X,t) = A(t) + B(t)\left(\frac{X}{L_0}\right)^2 + C(t)\left(\frac{X}{L_0}\right)^4 \tag{46}$$

One of the boundary conditions that can be applied to this expansion is that the end of the chain lies at the position of the right boundary

$$\begin{aligned} x(X = L_0,t) &= \int_0^{L_0} \lambda(X,t)\,dX \\ &= \left[A(t)X + \frac{B(t)}{3L_0^2}X^3 + \frac{C(t)}{5L_0^4}X^5\right]_0^{L0} \\ &= \left[A(t) + \frac{B(t)}{3}L_0 + \frac{C(t)}{5}\right]L_0 \end{aligned} \tag{47}$$

In addition, the right boundary position is related to the macro stretch by $x(X = L_0,t) = \tilde{\lambda}(t)L_0$. This condition reduces Eq. (47) to

$$\tilde{\lambda}(t) = A(t) + \frac{B(t)}{3} + \frac{C(t)}{5} \tag{48}$$

Because the global stretch is specified for all times, we can use this equation to eliminate one of the unknown functions. Equation (48) is solved for $A(t)$ and substituted into the assumed form of the deformation, Eq. (46), to obtain

$$\lambda(X,t) = \tilde{\lambda}(t) - \frac{B(t)}{3} - \frac{C(t)}{5} + B(t)\left(\frac{X}{L_0}\right)^2 + C(t)\left(\frac{X}{L_0}\right)^4 \tag{49}$$

The next step is to evaluate s in terms of these functions. Recasting Eq. (39) in terms of the stretch

$$s = \sqrt{\frac{1}{L_0}\int_0^{L_0}\left(\lambda-\tilde{\lambda}\right)^2 dX} = \sqrt{\widetilde{\lambda^2}-\tilde{\lambda}^2} \tag{50}$$

Our assumed form of λ is inserted into Eq. (50) and the integration is performed.

$$s = \sqrt{\frac{4}{45}B(t)^2+\frac{16}{105}B(t)C(t)+\frac{16}{225}C(t)^2} \tag{51}$$

In order to determine the unknown functions $B(t)$ and $C(t)$, we use the momentum equation in the original coordinate system. The momentum equation in this configuration, excluding finite extensibility effects, is

$$\rho_0\frac{\partial^2 x}{\partial t^2} = E_0\frac{\partial^2 x}{\partial X^2}\Big/\left(\frac{\partial x}{\partial X}\right) - f\frac{\partial x}{\partial t} \tag{52}$$

Equation (52) is rewritten in terms of the stretch

$$\rho_0\frac{\partial^2\lambda}{\partial t^2} = \frac{E_0}{\lambda}\frac{\partial^2\lambda}{\partial X^2} - \frac{E_0}{\lambda^2}\left(\frac{\partial\lambda}{\partial X}\right)^2 - f\frac{\partial\lambda}{\partial t} \tag{53}$$

With Eq. (49) substituted into this equation, we obtain two equations for the solution of the unknown functions. With the assumption that $\ddot{B}(t)$ and $\ddot{C}(t)$ are negligibly small, these equations are separated into two coupled ordinary differential equations

$$\dot{B}(t) = -\frac{E_0}{fL_0^2}\left(1350B(t)^2+900B(t)C(t)+540C(t)^2 - 2700C(t)\tilde{\lambda}(t)\right)\Big/\left(5B(t)+3C(t)-15\tilde{\lambda}(t)\right)^2 \tag{54}$$

and

$$\dot{C}(t) = \frac{E_0}{fL_0^2}\left[\left(3000B(t)^2+1950B(t)C(t)+900C(t)^2 - 2250B(t)\tilde{\lambda}(t)-4500C(t)\tilde{\lambda}(t)\right)\Big/\left(5B(t)+3C(t)-15\tilde{\lambda}(t)\right)^2\right]+5\dot{\tilde{\lambda}}(t) \tag{55}$$

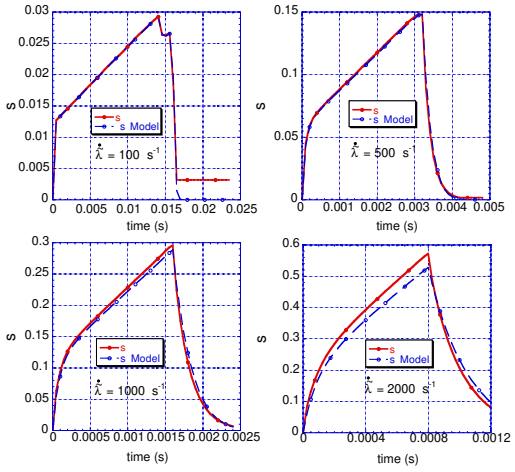

Figure 19. LOADING ONE: RESPONSE OF s FOR THE MODEL.

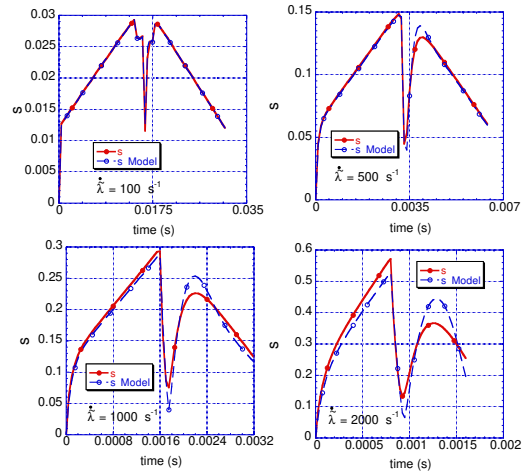

Figure 20. LOADING TWO: RESPONSE OF s FOR THE MODEL.

We have not found an analytical solution to this equation set. To demonstrate their relevance, we have implemented these equations into the computer code used in Section 4 and thereby obtained a solution for s that is compared with the value as computed by Eq. (39).

5.2 Numerical Solution and Comparison

In this section, we compare the approximation for s, Eq. (51), with the value of s obtained from the full solution of Eq. (39). In addition, the solutions for $B(t)$ and $C(t)$ are exhibited for simple loading cases, in order to assess the possibility of modeling these terms. The loadings and parameters for this investigation are the same as those for Section 4.

Figures 19 - 22 compare the evolution of s with that of the proposed model. The comparisons with the variations of s predicted by the code, shows that the model gives good representation for the non-equilibrium parameter if the deformations are kept simple. The plots show that the model solutions worsen with increasing stretch rate but still capture the essence of the

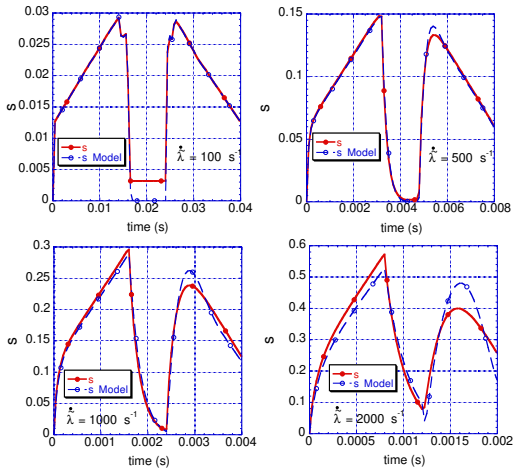

Figure 21. LOADING THREE: RESPONSE OF s FOR THE MODEL.

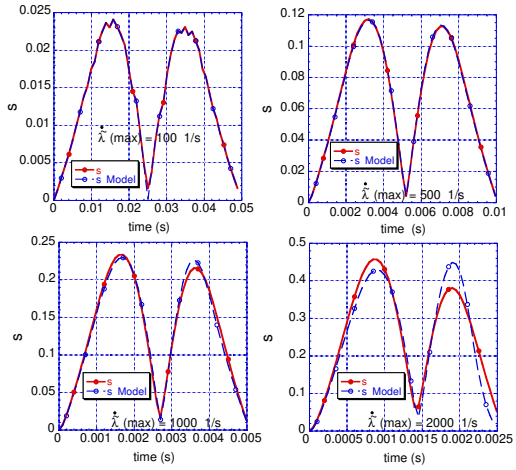

Figure 22. LOADING FOUR: RESPONSE OF s FOR THE MODEL.

parameter evolution very well.

It would be ideal if we could replace the ordinary differential equations for $B(t)$ and $C(t)$ with simple analytical forms. Figure 23 illustrates these functions as they vary with the time for four different loadings to see if this idea is plausible. At this stage, we see no simple way to parameterize the results of these calculations as functions of the driving conditions.

6 SUMMARY

We have developed the stochastic conservation equations for a single polymer chain embedded in other similar chains. The conservation equations are solved numerically in order to obtain the chain behavior for several loading paths and over a range of strain rates. With the use of a non-equilibrium parameter to help characterize these results, we develop a single chain constitutive model. The proposed model works well for stretch rates up to 10^3 s^{-1}, under the assumption of simple deformation in the chain. The single chain model has been used in a homogenization step to extract "continuum" behavior and then compare with experimental data. These results will be report in a follow-on paper.

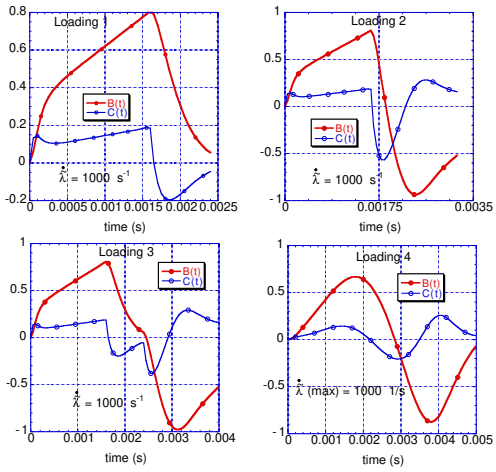

Figure 23. THE EVOLUTION OF THE FITTING FUNCTIONS $B(t)$ AND $C(t)$ VERSUS TIME FOR FOUR SIMPLE LOADING PATHS.

REFERENCES

E.M. Arruda and M.C. Boyce. A three-dimensional constitutive model for the large stretch behavior of rubber elastic materials. *J. Mech. Phys. Solids*, 41(2):389–412, 1993.

E.N. Harstad. *Stochastic Behavior of Polymers at High Strain Rates*. PhD thesis, University of New Mexico, 2001.

H.M. James and E. Guth. Theory of the elastic properties of rubber. *J. Chem. Phys.*, 11(10):455–481, 1943.

D.A. McQuarrie. *Statistical Mechanics*. Harper and Row, New York, 1973.

L.R.G. Treloar. *The Physics of Rubber Elasticity*. Clarendon Press Oxford, London, third edition, 1975.

G.E. Uhlenbeck and L.S. Ornstein. On the theory of the brownian motion. *Physical Review*, 36:823–831, 1930.

M.C. Wang and E. Guth. Statistical theory of networks of non-gaussian flexible chains. *J. Chem. Phys.*, 20(7):1144–1157, 1952.

Daniel Zwillinger, editor. *CRC Standard Mathematical Tables and Formulae*. CRC Press, New York, 1996.

ACKNOWLEDGMENT

Financial support for this work was provided through the Joint DOD/DOE Munitions Technology Development Program.